

REMOTE SENSING DATABASE PREPARATION FROM IRS DATA AND LULC CHANGE MONITORING OVER INDO-GANGETIC BASIN

D. R. Rajak*, M. R. Bhuyan, M. P. Oza, N. K. Patel and J. S. Parihar

Agricultural Resources Group, RESIPA
Space Applications Centre, Ahmedabad-380015, India.
(rajakdr, sac9271, markand, nkpatel, jsparihar)@sac.isro.gov.in

KEY WORDS: Remote Sensing Database, IRS Data, Haze Compensation, Land Use / Land Cover Changes, Projection Scheme

ABSTRACT:

This paper describes the methodology developed and implemented for Remote Sensing DataBase (RSDB) preparation from multi-temporal and multi-sensor data from Indian earth observation satellites. The characteristics of the RSDB prepared over parts of Indo-Gangetic Basin and Central India (IGB&CI) are summarised. An approach for extraction of long term (1988-89 to 2004-05) Land Use / Land Cover (LULC) changes using RSDB over selected sites is demonstrated. Design of analysis framework and selection of a suitable projection scheme with optimization of scale factors has been discussed. The major components of procedure are multi-date RS data geo-referencing, radiometric normalization, top of atmosphere (TOA) reflectance images preparation, multi-image compositing and mosaicing. An RSDB for three rabi (winter) seasons i.e. 1988-89 (226 IRS 1A LISS-II quadrants), 1993-94 (251 IRS 1B LISS-II quadrants) and 2004-05 (three bi-monthly sets, 170 IRS P6 AWiFS quadrants) has been prepared over IGB&CI. Long term LULC changes in terms of increase or decrease in area under agriculture, urban, forest and water bodies have been mapped and quantified using temporal composite images of 1988-89 and 2004-05 rabi seasons. Increase in agricultural area due to conversion of water bodies into crop area (parts of Rajasthan) of the order of 6021 ha (overall increase in crop area from 22383 ha to 43596 ha) and intensification of agriculture into river flood plains (parts of Punjab) of the order of 38.2 percent (of the study area) have been mapped. On the other hand, decrease in agriculture and other land cover area due to urban sprawl has been detected and mapped in the surrounding of Agra town in Uttar Pradesh.

1. INTRODUCTION

The availability of multi-temporal Remote Sensing (RS) data has added an unprecedented dimension to the monitoring of spatial information over time. The extensive spatial information about earth, its environment and natural resources, with such clarity and accuracy was never available before. World wide efforts are being made to prepare temporal RSDBs to extract the required information at various scales from local and regional to global. Information on land cover and land cover changes is one of the most important contributions of such datasets. The emergence of global environmental issues addressed by the International Geo-sphere Bio-sphere Programme (IGBP), United Nation's Framework Convention of Climate Change (UNFCCC), United Nation's Convention for Combating Desertification (UNCCD), the Kyoto Protocol, the Biodiversity Convention, Global Observing Systems and other international policy instruments have brought a new, critical requirement for land cover information at many scales, from landscape to global. A major effort is involved in transforming raw RS data collected by different sensors into a format from which land cover information can be extracted. To meet this requirement, a need of a well-designed RS database has been accepted globally. The NASA's Earth Observation System (EOS) Pathfinder Programme is aimed at developing improved long-term satellite data products for global change research. In PAL (Pathfinder AVHRR Land) - I Programme, initially a RS database using AVHRR data from 1982 to 1994 at a spatial resolution of 8 km was created (Agbu and James, 1994). A subsequent related project (PAL-II) was taken up to provide global 1 km data (initially for 1992-1993 and then for 1995-1996). The availability of these datasets has been pivotal in the

development of techniques to derive global and regional land cover products from satellite data. Land Surface Reflectance (LASUR) and Global Vegetation Index (GVI) are some other datasets derived from AVHRR data. The NASA Moderate Resolution Imaging Spectro-radiometer (MODIS) land science team concluded that a global land 1-km AVHRR data set is crucial to develop algorithms for several land products for the Earth Observing System (EOS) (Running *et al.*, 1993). The SPOT - VEGETATION database at a spatial resolution of 1 km is also being produced regularly by Belgian institute VITO (Flemish Institute for Technological Research).

India started acquiring RS data from Landsat in July 1979. With the launch of its own satellite (Indian Remote Sensing Satellite i.e. IRS 1A) a new era of RS data acquisition for natural resources started in 1988. The RS data collected through different sensors onboard various satellites from polar to geo-synchronous orbits, has been used for many applications like agriculture, environment, water resources, forestry, town planning, hydrology, meteorology, oceanography etc. The first attempt to prepare a systematic temporal RSDB using earth observation (EO) data from Indian Remote Sensing Satellites has been made at Space Applications Centre in 2003. In the first phase of the study, an RSDB over parts of IGB&CI has been prepared for 1988-89, 1993-94 and 2004-05 rabi seasons (Rajak and Dadhwal, 2003).

This paper describes the methodology adopted for RSDB preparation from multi-temporal and multi-sensor Indian EO data, characteristics of the RSDB over parts of IGB&CI and extraction of long term LULC changes over selected sites. Long term LULC changes in terms of increase or decrease in area of

* Corresponding author: rajakdr@sac.isro.gov.in
: rajakdr@yahoo.com

agricultural, urban, forest and water bodies have been mapped for selected sites and quantified using 1988-89 and 2004-05 rabi seasons data. Increase in agricultural area due to conversion of low lying water bodies into crop area, intensification of agriculture into river flood plains and decrease in agriculture area due to urban sprawl were detected, quantified and mapped.

2. STUDY AREA AND DATASET

While the overall aim was to prepare an RSDB over India, in the first phase Indo-Gangetic Basin and parts of central India were taken up as study area. Indo-Gangetic Basin represents international importance as a major source of food grain production in Indian subcontinent and is associated with large human impact.

The basic data used included satellite remote sensing data with ancillary data like Survey of India topographic maps for base images preparation and India boundary coverage for data analysis framework preparation. The satellite data included 477 IRS 1A and 1B LISS-II quadrants (October to April for 1988-89 and 1993-94 rabi seasons), 227 IRS LISS-III scenes (November 2001 to March 2002 for base images) and 170 IRS P6 AWiFS quadrants (October 2004 to March 2005).

3. METHODOLOGY

The methodology of RSDB preparation and long-term LULC change detection and mapping may be summarised under the following steps:

3.1 Data Analysis Framework

The study area was covered in multiple tiles, sub-tiles and chips. The basic RSDB unit size is "tile" of usual size of 4°x4°. Each tile is usually further divided into sub-tiles (2°x2°) and chips (1°x1°). To analyse RS data with spatial resolution coarser than 250 m for whole country, Albers Conic Equal Area (ACEA) projection with two standard parallels at 28° N and 12° N (central meridian at 78° E, Latitude of origin at 20° N, False Easting and Northing both 2000000 m with Everest ellipsoid), has been chosen. To use finer resolution data, analysis has to be carried out in parts and then results are obtained by integration. To mosaic the images seamlessly, the distortions in adjoining images introduced due to projection should be minimised. Keeping in mind such criteria, TM projection (secant) with Everest ellipsoid has been chosen for RS data (spatial resolution of 25 to 250 m) analysis. Scale factors are optimised for 4° x 4° working tiles (Appendix A) at reference latitude (Rajak *et al.*, 2002).

The approximate formula for the computation of the scale factor in the TM projection with cylinder being secant to the datum surface (Bugayevskiy and Snyder, 1995) is as follows:

$$m_p = m_0 \{1 + (d^2 / 2R^2) + (d^4 / 24R^4) + (d^6 / 720R^6)\} \dots \quad (1)$$

where m_0 = scale factor assigned to the central meridian
 d = scaled distance on the projection from the central meridian
 m_p = scale factor at the point in question
 R = mean radius of the Earth, given by:

$$R = (M * N)^{1/2} = N / (1 + \eta^2)^{1/2} \dots \quad (2)$$

The radius of curvature of the meridian (M) at the point in

question is given by:

$$M = a * (1 - \epsilon^2) / [(1 - \epsilon^2 * \sin^2 f)^{3/2}] \dots \quad (3)$$

where a = the semi major axis of the meridional Earth ellipsoid
 = the equatorial radius
 b = the semi minor axis of the meridional Earth ellipsoid
 = the polar radius
 f = the geodetic latitude at the point
 ϵ = the first eccentricity of the Earth ellipsoid, given by:

$$\epsilon = [(a^2 - b^2) / a^2]^{1/2} \dots \quad (4)$$

The radius of curvature (N) in the direction of the prime vertical perpendicular to the direction of meridian at the point in question is given by:

$$N = a / [(1 - \epsilon^2 * \sin^2 f)^{1/2}] \dots \quad (5)$$

$$\eta = \epsilon' * \cos(f) \text{ and } \epsilon' = (a/b)^2 - 1 \dots \quad (6)$$

ϵ' is the 2nd eccentricity of the Earth ellipsoid and f is the geodetic latitude at the point.

3.2 Base Images Preparation

The objective of this task was to prepare geographically consistent base images across the study area to which the images of other years and other dates were georeferenced. The task was accomplished by map-to-image registrations with root mean square accuracy better than one pixel of image.

The images from IRS 1D LISS-III were selected for this purpose. Multi-temporal images (227) were geo-referenced to prepare the base tiles covering almost 90 percent of Indian land mass. Survey of India (SOI) topographic maps at 1:50 000 scales were used to derive the geographic coordinates of the Ground Control Points (GCPs). Well distributed GCPs between map and image were identified and tile-wise transformations were developed to register IRS LISS-III scenes with SOI maps. The absolute geo-metric error for each base tile in terms of root mean square error was within one pixel of LISS-III.

3.3 Multi-sensor Data Calibration and Multi-date Geo-referencing

To take into account the variation due to different sensors a basic calibration of conversion of digital numbers (DNs) to radiance at sensor was carried out. Radiance at sensor (L) was calculated using the calibration coefficients for the sensors by following formula:

$$L = L_{\min} + (DN_i - DN_{\min}) * L_{\max} / (DN_{\max} - DN_{\min}) \dots \quad (7)$$

The values of L_{\min} for all the bands in both the sensors are zero and values of L_{\max} for LISS-II (IRS 1A and 1B) and AWiFS (IRS P6) are given in table 1. The radiance values are multiplied by 1000 and stored in 16-bit format. Geo-referencing of multi-date and multi-sensor data is carried out by image to image co-registrations. The base images prepared from IRS LISS-III were taken as master images and multi-date IRS LISS-II and IRS AWiFS calibrated radiance images were registered with master images using second order polynomial transformation with uniform distribution of GCPs over both the images. A relative geo-metric accuracy requirement was kept high (± 0.5 pixels of coarser data).

3.4 In-scene Haze Normalisation

Extensive literature is available on atmospheric theory and potential effects of atmosphere on remote sensing. There are limited studies that deal with the practicality of compensating for spatially varying haze in an image. The usual approach is to locate targets with very low signal in the scene and to estimate local aerosol optical depth using these targets.

Sr No	Band	IRS 1 A LISS-II (L_{max})*	IRS 1 B LISS-II (L_{max})*	IRS P6 AWiFS (L_{max})*
1	Blue	16.644	14.069	-
2	Green	23.132	22.653	52.3
3	Red	18.261	18.019	40.8
4	NIR	16.418	16.445	28.4
5	SWIR	-	-	4.65

* L_{max} in mw/sq.cm/str/micron

Table 1: The values of L_{max} for LISS-II and AWiFS sensors

Liang *et al.* (1997) used such an approach to generate a low-frequency haze mask. In a visual inspection of the tasselled cap transformation to Landsat TM, it was observed that the dominant response of its fourth component appeared due to atmospheric haze (Crist and Ciccone, 1984). On this basis, Richter (1996) corrected a TM sub-scene for atmospheric effects. Similarly, based on the observation that the atmospheric haze tends to obscure high spatial frequency variations in the recorded signal, Du *et al.* (2002) developed a wavelet transform based approach to correct multiple images of the same scene. Based on the fact that visible bands exhibit a highly correlated response to a wide range of thematic classes under clear sky conditions but differing levels of radiometric sensitivity to haze, Zhang *et al.* (2002) developed a Haze Optimised Transform (HOT) that provided superior performance in the detection of haze compared to the tasselled cap transform.

For analysing data at national level, a haze compensation methodology is essential. The methodology should be image based, since ancillary atmospheric information (aerosol type, optical depth etc) for historical data would not be available. The study under consideration adopted the HOT based in-scene haze compensation approach. In this approach, the haze free regions of a scene are visually identified and the radiance values over such areas are used to define “clear line” on scatter plots as shown in figure 1. The orthogonal displacement of each pixel from the “clear line” is then measures by HOT:

$$HOT = GREEN * \sin T - RED * \cos T \quad \dots \quad (8)$$

where, GREEN and RED are radiance values of pixel in green and red bands, and T is the angle of the slope of the regression line (clear line) in the green band versus red band spectral space. The HOT image prepared in this manner characterises the spatial distribution of haze contamination. The pixels under thin haze are then subjected to haze compensation. No haze compensation is made for the pixels which are either under haze free condition or thick haze/cloud condition.

3.5 Data Quality Flag Generation

Based on the statistics of haze free regions and thin haze regions, thresholds are decided to mark the pixels which are to be subjected for haze compensation. The pixels with lower than lower haze threshold HOT values are considered as haze free

and no compensation needed for those pixels and a quality flag 0 (zero) is assigned. The pixels with upper haze threshold HOT values are considered as cloudy pixels and a quality flag 2 is assigned. The haze compensation is carried out for the pixels with HOT values lying between lower haze threshold and upper haze threshold and a quality flag 1 is assigned.

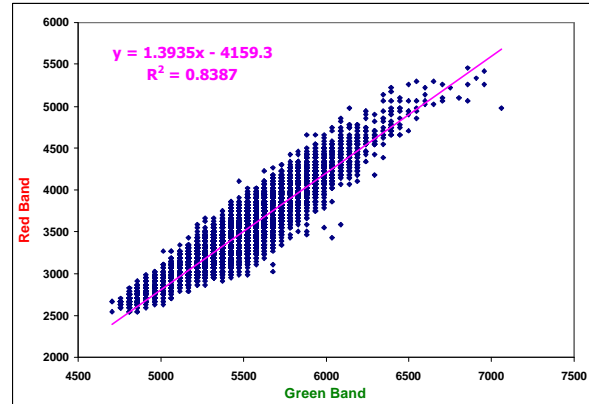


Figure 1: “Clear Line” in Green versus Red bands spectral space

3.6 Solar Zenith Angle Image preparation

Solar zenith angle (θ) at each pixel location was calculated by the following formula customised for spatial image analysis (SWAT, 2002):

$$\cos(\theta) = \frac{\sin(T) * \sin(\phi) + \cos(T) * \cos(\phi) * \cos((180 - GMT) * 15 - \lambda)}{\cos((180 - GMT) * 15 - \lambda)} \quad \dots \quad (9)$$

where,

- T = Sun Declination Angle
- ϕ = Latitude of pixel location (from image geographic coordinate)
- λ = Longitude of pixel location (from image geographic coordinate)
- GMT = Greenwich Mean Time of Image Acquisition (from image metadata) (hours)

The Sun declination angle (T) is calculated by:

$$\sin(T) = 0.4 * \sin(2 * p * (DOY - 82) / 365) \quad \dots \quad (10)$$

where,

DOY = Day of the year from first January

3.7 Top-of-atmosphere (TOA) Reflectance Image Preparation

The reflectance image i.e. TOA reflectance (ρ) image was prepared from at sensor radiance image with solar zenith angle and exo-atmospheric irradiance correction, by the following formula:

$$\rho = (p * d^2 * L) / E_0 * \cos(\theta) \quad \dots \quad (11)$$

where,

- L = at sensor radiance (from equation 7)
- E_0 = Exo-atmospheric irradiance for the band
- θ = Sun zenith angle (from equation 9)
- d = mean Sun-Earth distance, calculated by:

$$d^2 = 1/(1+0.033*\cos(2*p*DOY/365)) \quad \dots \quad (12)$$

The values of exoatmospheric irradiance for different bands in IRS satellite sensors have been worked out by Pandya *et al.* 2006.

3.8 Multi-date Compositing and Mosaicing

To obtain a synthesised cloud free view of any complete tile or sub-tile from all available scenes within selected time period, a pixel to pixel compositing and mosaicing process is performed. The compositing algorithm chosen is a combination of “best quality flag” and the Maximum Value Composite (maximum NDVI). For a given pixel having been viewed several times, the selected TOA reflectance in the final composite image corresponds to the viewing having the best quality flag (0 better than and 1 better than 2) and maximum NDVI value. Cloudy, bad quality or interpolated views are excluded, if possible.

3.9 Vegetation Index Image Preparation

The NDVI i.e. the ratio (NIR-RED) / (NIR+RED) values are calculated for each pixel from TOA reflectance values in composite image. The NDVI values are scaled (100 + 100 * NDVI) and stored in 8-bit format.

3.10 LULC Change Detection and Mapping

Digital change detection is the process that helps in determining the changes associated with land use and land cover properties with reference to geo-registered multi-temporal RS data. It helps in identifying changes between two (or more) dates that is uncharacterised of normal variation. Change detection is useful in many applications such as land use changes, rate of afforestation/deforestation, coastal change, urban sprawl, and other cumulative changes through spatial and temporal analysis techniques such as GIS (Geographic Information System) and RS along with digital image processing techniques.

The forest inventory/survey using high resolution RS data from IRS satellites supplemented with extensive field checking or sampling has been categorised under “high reliability” class (Source:http://www.fao.org/docrep/field/385907.htm#P258_14962) in United Nation’s Food and Agriculture Organisation (FAO) Global Forest Resources Assessment.

In the study presented here, the land-cover change detection approach is based on a comparison of the temporal spectral patterns of land cover classes for successive years - e.g. a pattern of vegetation index. When the time trajectory or temporal pattern of the spectral indicator (like NDVI) over a particular pixel departs from the pixel’s reference time trajectory, a change in land-cover is detected.

4. RESULTS AND DISCUSSION

The RS data analysis framework was designed in terms of tiles (4°x4°) and sub-tiles (2°x2°). The base composite images over sub-tiles were prepared with root mean square errors less than one pixel. The multi-date, multi-year and multi-sensor RS data was geo-referenced with very high relative geometric accuracy of 0.5 pixels. The calibrated radiance and TOA reflectance sub-tiles images from IRS LISS-II are available at 50 m pixel size while TOA reflectance tiles images from IRS P6 AWiFS are at 100 m pixel size. The radiance and TOA reflectance images are multiplied by 10³ and 10⁴, respectively and the scaled images are stored in 16 bit unsigned data formats. The date indices are

stored in 16-bit format while quality flag values are stored in 8-bit formats. The layers available in RSDB are listed in Table 2.

Band	Description	Band	Description
1	Calibrated Blue Radiance *	8	Apparent Red Reflectance
2	Calibrated Green Radiance	9	Apparent NIR Reflectance
3	Calibrated Red Radiance	10	Apparent SWIR Reflectance **
4	Calibrated NIR Radiance	11	Quality flag (Haze/Cloud)
5	Calibrated SWIR Radiance **	12	Date Index
6	Apparent Blue Reflectance *	13	Solar Zenith Angle
7	Apparent Green Reflectance	14	NDVI

* Available in LISS-II derived RSDB

** Available in AWiFS derived RSDB

Table 2: Characteristics layers in RSDB

Figure 2 shows temporal composite images from IRS LISS-II (rabi 1988-89), IRS AWiFS (rabi 2004-05, December 2004-January 2005) and a LULC change image derived from the two composite images over a selected study site. The geographic area of the study site was 102510 ha and it is located over parts of western Rajasthan in India. The major changes are observed in terms of overall increase in agricultural crop area and decrease in water bodies. The rabi crop area in 2004-05 was 43596 ha in comparison to 22383 ha in 1988-89 i.e. an increase by 95 percent of the crop area. The area under water bodies reduced to 918 ha in 2004-05 from 9720 ha of 1988-89 i.e. a reduction by 91 percent of water bodies’ area. The LULC change matrix is shown in table 3.

Season	Rabi 2004-05			
	Classes	Crop	Water	Other
Rabi 1988-89	Crop	17046	171	5166
	Water	6021	351	3348
	Other	20529	396	49482

Table 3: LULC Change matrix (land cover area in hectares)

The LULC change analysis for other selected sites spread over the study area was performed and the changes were quantified and the spatial mapping of LULC changes was carried out. The major LULC change of 64.3 percent increase in urban area surrounding Agra city from 1988-89 to 2004-05 was observed and mapped. This increase was at the cost of reduction in agricultural and other land covers. From the analysis of another site over parts of Punjab, an extensive increase in the agricultural area was identified and mapped. The crop area increased due to advancement of agriculture over the vast flood plains of river Satluj. The increase in agricultural area was of the order of 38.2 percent.

5. CONCLUSIONS

A methodology for preparation of an RSDB from IRS sensors was developed and implemented. A RS analysis framework and TM (secant) projection scheme with optimised scale factors for 4°x4° tiles were designed for India. An Indian RSDB over parts of Indo-Gangetic Basin and Central India for three rabi seasons was prepared.

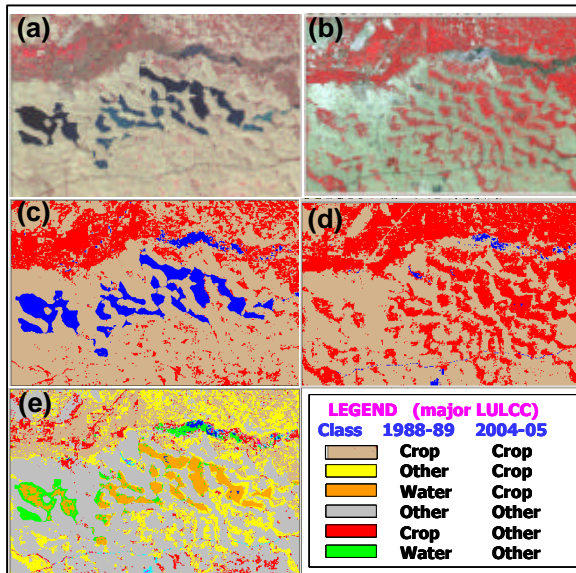


Figure 2: Temporal composite images (a: rabi 1988-89, b: rabi 2004-05), classified images (c: 1988-89, d: 2004-05) and LULC change image (e) for a selected site over parts of Rajasthan, India.

The RSDB for 1988-89 and 1993-94 was prepared from the analysis of more than 477 quadrants of IRS 1A and IRS 1B LISS-II sensors while for 2004-05 was prepared from 170 quadrants of IRS P6 AWiFS sensor. The image processing modules for geometric registration, DN to radiance conversion, radiometric normalisation (in-scene haze compensation by HOT), quality flag and date index generation, solar zenith correction, TOA reflectance image preparation and multi-date compositing (best quality flag and maximum NDVI) and mosaicing were finalised and implemented. The applications of RSDB for LULC change detection, quantification and spatial mapping were demonstrated over selected sites in the study area. The decrease in water bodies and flood plain areas due to increase in agricultural area was observed and mapped over two selected sites in parts of Rajasthan and Punjab; while decrease in agricultural area was found because expansion of urban area surrounding the Agra city in Uttar Pradesh.

References

- Agbu, P.A., and James, M. E., 1994. The NOAA/NASA Pathfinder AVHRR land data set user's manual. Greenbelt, MD: Goddard Distributed Active Archive Centre Publications, GCDG.
- Bugayevskiy, L. M. and Snyder, J. P., 1995. Map projections - A reference manual. Taylor & Francis Ltd, 4 John St, London.
- Crist, E. P. and Ciccone, R. C., 1984. A Physically-based Transformation of Thematic Mapper Data - the TM Tasselled Cap. *IEEE Transactions on Geoscience and Remote Sensing*, 19, pp. 3141 - 3168.

Du, Y., Guindon, B., and Cihlar, J., 2002. Haze Detection and Removal in High Resolution Satellite Image with Wavelet Analysis. *IEEE Transactions on Geoscience and Remote Sensing*, 40, pp. 210 - 217.

http://www.fao.org/docrep/field/385907.htm#P258_14962

Liang, S., Fallah-Adl, H., Kalluri, S., Jaja, J., Kaufman, Y. J., and Townshend, J. R. G., 1997. An Operational Atmospheric Correction Algorithm for Landsat Thematic Mapper Imagery over the Land. *Journal of Geophysical Research*, 102, pp. 17 173 - 17 186.

Pandya, M. R., Singh, R. P., Chaudhari, K. N., Murali, K. R., Kirankumar, A. S., Dadhwal, V. K. and Parihar, J. S., 2006. Spectral characteristics of sensors onboard IRS-1D and P6 satellites: Estimation and their influence on reflectance and NDVI measurement (to be published).

Rajak, D.R, Oza, S. R., Oza, M. P. and Dadhwal, V. K., 2002. Selection of map projections for crop monitoring spatial database. Scientific Note, Space Applications Centre, Ahmedabad, India, RSAM/SAC/RSDB/SN/01/2002.

Rajak, D. R. and Dadhwal, V. K., 2003. Preparation of a Multi-temporal Remote Sensing Database (Phase I: Parts of Indo-Gangetic Basin and Central India). Project Proposal: RSAM/SAC/RSDB/PP/01/2003, Space Applications Centre, Ahmedabad, India.

Running, S. W., Justice, C. O., Salomonson, V. V., Hall, D., Barker, J., Kaufmann, Y. J., Strahler, A. H., Huete, A. R., Muller, J.-P., Vanderbilt, V., Wan, Z. M., Teillet, P. M., and Carneggie, D., 1993. Terrestrial remote sensing science and algorithms planned for the Moderate Resolution Imaging Spectrometer (MODIS) of the Earth Observing System (EOS). *The International Journal of Remote Sensing*, 15, pp. 3587-3620.

Richter, R., 1996. Atmospheric correction of satellite data with haze removal including a haze / clear transition region. *Computer and Geosciences*, 22, pp. 675-681.

SWAT, 2002. Soil and Water Assessment Tool - Theoretical Documentation: Version 2000, Water Resources Institute, College Station, Texas, TWRI Report TR-191, pp. 48.

Zhang, Y., Guindon, B., and Cihlar, J., 2002. An Image Transform to Characterize and Compensate for Spatial Variations in Thin Cloud Contamination of Landsat Images, *Remote Sensing of Environment*, 82, pp. 173-187.

Acknowledgements

The authors acknowledge the encouragement provided by Dr. R. R. Navalgund, Director, Space Applications Centre, Ahmedabad in carrying out this study.

Appendix A: T M (secant) projection parameters optimised for 4° x 4° tiles over India

Tile No.	N-S Extent		E-W Extent		C. Merid. (Deg.)	Ref. Lat. (Deg.)	Scale Factor (at c. Merid.)	F. East. (m)	F. North. (m)	Remark
	Lat1	Lat2	Long1	Long2						
1	6	10	92	94	93	8	0.999702	300000	300000	A&N
2	10	14	92	95	93	12	0.999709	300000	300000	A&N
3	8	12	72	76	74	10	0.999705	300000	300000	L&M
4	8	12	76	80	78	10	0.999705	300000	300000	KER,TN, KAR
5	12	16	73	76	74	14	0.999714	300000	300000	KAR,KER,MAH,GOA
6	12	16	76	80	78	14	0.999714	300000	300000	KAR,TN,AP
7	12	16	80	82	82	14	0.999714	300000	300000	AP,TN
8	16	20	72	76	74	18	0.999725	300000	300000	MAH,KAR
9	16	20	76	80	78	18	0.999725	300000	300000	MAH,KAR,AP
10	16	20	80	84	82	18	0.999725	300000	300000	AP,CHH,ORI
11	18	20	84	87	86	19	0.999728	300000	300000	ORI,AP
12	20	24	68	72	70	22	0.999738	300000	300000	GUJ
13	20	24	72	76	74	22	0.999738	300000	300000	GUJ,MAH,RAJ,MP
14	20	24	76	80	78	22	0.999738	300000	300000	MAH,MP
15	20	24	80	84	82	22	0.999738	300000	300000	MAH,CHH,MP,ORI
16	20	24	84	88	86	22	0.999738	300000	300000	ORI,JHA,WB
17	21	25	88	90	89	23	0.999742	300000	300000	WB
18	24	28	68	72	70	26	0.999754	300000	300000	RAJ,GUJ
19	24	28	72	76	74	26	0.999754	300000	300000	RAJ,GUJ,MP
20	24	28	76	80	78	26	0.999754	300000	300000	RAJ,MP,UP
21	24	28	80	84	82	26	0.999754	300000	300000	MP,UP,JHA,BIH
22	24	28	84	88	86	26	0.999754	300000	300000	UP,BIH,JHA,WB
23	28	32	72	76	74	30	0.999772	300000	300000	RAJ,HAR,PUN
24	28	32	76	80	78	30	0.999772	300000	300000	HAR,DEL,PUN,HP,UTT,UP
25	28	31	80	82	81	29	0.999767	300000	300000	UP,UTT
26	32	36	73	76	74	34	0.999791	300000	300000	J&K,HP,PUN
27	32	36	76	80	78	34	0.999791	300000	300000	HP,J&K
28	36	38	72	77	75	37	0.999806	300000	300000	J&K
29	25	29	88	91	89	27	0.999758	300000	300000	WB,SIK,ASS,MEG
30	22	26	91	95	93	24	0.999746	300000	300000	MEG,TRI,MIZ,ASS,MAN,NAG
31	26	29	91	94	93	27	0.999758	300000	300000	ASS,ARU
32	26	30	94	98	96	28	0.999763	300000	300000	ARU,ASS,NAG

(Source: Rajak *et al.*, 2002)

- o North-South and East-West extents i.e. (Lat1, Lat2) and (Long1, Long2) of tiles are within 4° latitude and longitude, respectively.
- o C. Merid. is central meridian for the tile
- o Ref. Lat. is reference latitude for the tile
- o The above calculations are based on Everest ellipsoid having semi-major radius = 6377276.3 m and semi-minor radius = 6356075.4 m.